DOI: 10.1021/ma900781c

Macromolecules
ARTICLE

Nanoscale Phase Separation of Sulfonated Poly(arylene ether sulfone)/ Poly(ether sulfone) Semi-IPNs for DMFC Membrane Applications

Yo Han Kwon,[†] Sung Chul Kim,*[,†] and Sang-Young Lee*[,‡]

[†]*Department of Chemical and Bimolecular Engineering, KAIST, 373-1 Guseong-dong, Yuseong-gu, Daejeon 305-701, Republic of Korea, and* [‡]*Department of Chemical Engineering, Kangwon National University, 192-1 Hyoja-dong, Chuncheon, Kangwon-do 200-701, Republic of Korea*

Received April 10, 2009; Revised Manuscript Received June 12, 2009

ABSTRACT: Unprecedented improvement in the selectivity (the ratio of proton conductivity to methanol permeability) of DMFC (direct methanol fuel cell) membranes has been demonstrated with a value roughly 16 times higher than that of Nafion117 having been achieved. The novel morphology of semi-interpenetrating polymer network (semi-IPN) membranes characterized by nanometer-sized domains as well as well-developed phase cocontinuity is a key factor in enabling such notable progress, which has not been seen in conventional microscale phase separation. The semi-IPN membranes (sIPN-100) consisted of a hydrophilic component acting as a proton conductor, that is, acrylate-terminated fully sulfonated poly(arylene ether sulfone) oligomers (acSPAES-100, degree of sulfonation = 100%), and a hydrophobic component functioning as a methanol barrier, that is, poly(ether sulfone) copolymers (RH-2000). We determined the nanoscale phase separation of sIPN-100 by deliberately controlling the kinetics (the change of solvent-evaporation conditions) as well as the thermodynamics (shift of the phase separation boundary to the lower concentration of solvent in the phase diagram, mostly driven by the low molecular weight and the low hydrophilicity of acSPAES-100). Finally, the influence of this unique morphology on the membrane transport properties including the proton conductivity, the methanol permeability, and, more notably, the selectivity, was systematically investigated.

Introduction

Owing to their high thermal stability, excellent mechanical strength, and strong resistance to membrane decomposition in an acidic water medium, polyarylene-based ionomers with sulfonic acids have been investigated as a promising alternative to Nafion.[1−6] However, most of these ionomers exhibit higher methanol permeability and water uptake than Nafion, leading to low selectivity. The methanol crossover through polyelectrolyte membranes has caused severe problems that bring about loss of fuel, poor fuel efficiency, voltage drop, and excess thermal load in the cells.[7−9] To overcome these drawbacks, a variety of approaches have been attempted, including organic−inorganic hybrid membranes,[10−12] cross-linking-network membranes,[13−15] and polymer−polymer blend membranes.[16−19] Among them, notably, blend membranes with a cocontinuous morphology have drawn strong attention because of their unique phase structure. In the blend membranes, the morphology is considered to be a crucial factor to control the methanol crossover as well as the proton conductivity.[17−19]

The aim of this study is to develop cocontinuous morphology with nanoscale phase-separated structures. This has never been achieved in blend membranes and is expected to provide breakthroughs in DMFC membrane performance. Although previous studies on blend membranes reported cocontinuous morphology, the average domain size has been limited to a range of submicrometers and has not yet been achieved on the nanoscale.[16−19] It is known that the membrane transport properties including methanol crossover and proton conductivity strongly depend on the fraction and the state of water, indicating that they can be improved by controlling the hydrophilic domain size in the blend membranes.[17−19] This underlines the fact that nanoscale control of phase separation could be a novel approach to overcome the technical limitations of conventional approaches.

Nanoscale phase separation can be realized by controlling the kinetics as well as the thermodynamics. First, to allow the phase separation to be frozen in the early stage of spinodal decomposition, the boundary of phase separation shifts to the lower concentration of solvent in the phase diagram. This is driven by control of the molecular weight and the polarity of the blend components. It is known that low molecular weight and a reduction in the polarity difference between blend components can contribute to enhanced miscibility in blend systems.[21,22] On the basis of this background, as a blend membrane, a semi-IPN consisting of cross-linkable sufonated oligomers with bulky pendant ions and nonsulfonated polymers was prepared. As a hydrophilic component acting as a proton conductor, acrylate-terminated and fully sulfonated poly(arylene ether sulfone) oligomers (acSPAES-100, degree of sulfonation = 100%) with tetrabutylammonium ions were synthesized, where bulky pendant ions as well as low molecular weight are introduced to deliver improved miscibility with the nonsulfonated polymers. To provide acSPAES-100 with proton-conducting activity, after completing the phase separation of semi-IPN membranes, the tetrabutylammonium ions in acSPAES-100 were substituted with protons from sulfuric acid (H_2SO_4). As a hydrophobic component functioning as a methanol barrier, poly(ether sulfone) copolymers (RH-2000) were employed. Meanwhile, for the purpose of controlling the phase separation kinetics, the solvent-evaporation conditions during the membrane preparation were varied before UV-cross-linking is applied to freeze the blend morphology.

Experimental Section

Semi-Interpenetrating Polymer Network Membrane Preparation. The semi-IPN membranes (sIPN-100) were prepared by

*Corresponding authors. (S.C.K.) Tel: + 82 42 350 3914. Fax: + 82 42 350 3910. E-mail: kimsc@kaist.ac.kr. (S.-Y.L.) Tel: + 82 33 250 6338. Fax: + 82 33 250 6338. E-mail: syleek@kangwon.ac.kr.

 Published on Web 07/02/2009

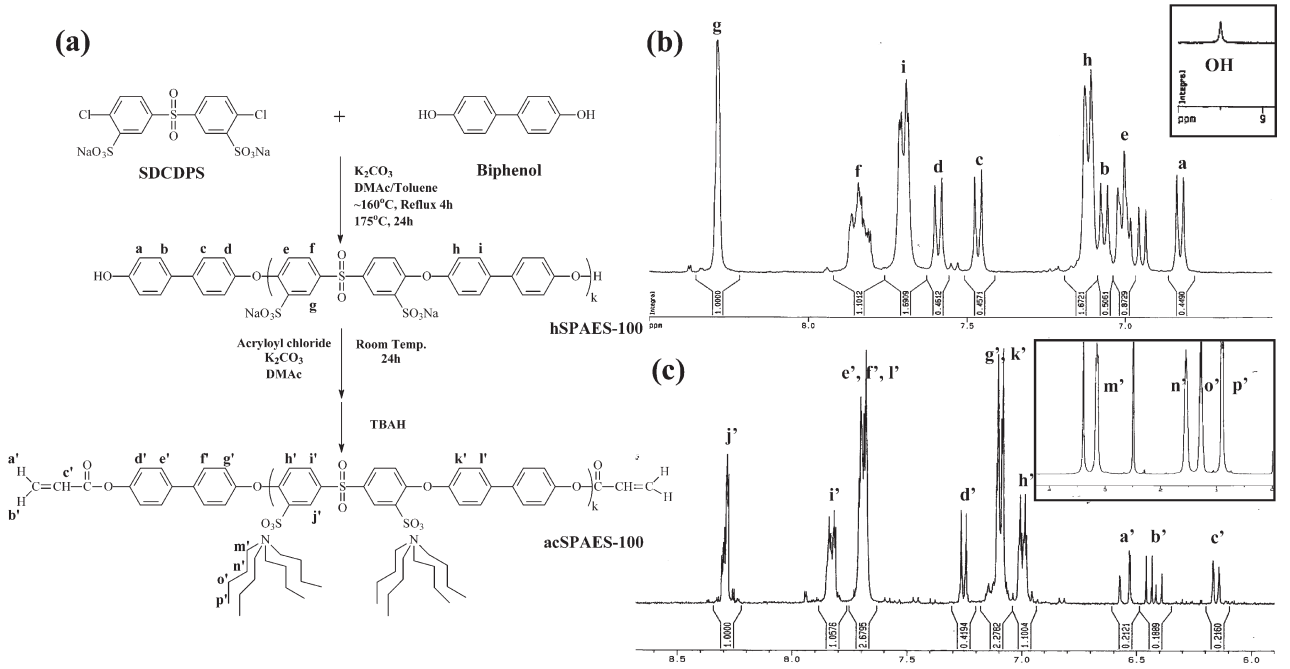

Figure 1. Synthesis and characterization of fully sulfonated poly(arylene ether sulfone) oligomers. (a) Synthetic scheme of hSPAES-100 (sodium form) and acSPAES-100 (ammonium form). ^{1}H NMR spectra (DMSO-d_6 as a solvent) of (b) hSPAES-100 (sodium form) and (c) acSPAES-100 (ammonium form).

following two steps: (1) synthesis of cross-linkable sulfonated oligomers with bulky pendent ions and (2) preparation of sIPN-100. Figure 1a shows the synthetic scheme of hydroxyl-terminated fully sulfonated poly(arylene ether sulfone) oligomers (hSPAES-100, degree of sulfonation = 100%) as an intermediate product and acrylate-terminated fully sulfonated poly(arylene ether sulfone) oligomers (acSPAES-100, degree of sulfonation = 100%) as a final product. The hSPAES-100 was synthesized by an aromatic nucleophilic substitution step growth polymerization, where the molecular weight was controlled at 3000 g/mol. It was synthesized by reacting 3,3′-disulfonated 4,4′-dichlorodiphenylsulfone (SCDPS, 12.36 mmol) and 4,4′-biphenol (BP, 15.00 mmol) and potassium carbonate (18.00 mmol). After the addition of anhydrous DMAc and toluene, the temperature was gradually increased to 175 °C, and then the reaction was allowed to proceed for 24 h, where reaction compounds became viscous and brownish. After the resulting solution was cooled to room temperature, this solution was diluted with DMAc and then filtrated by glass filter to remove salts. The sulfonated oligomers were precipitated via coagulation in IPA, and the precipitated oligomers were washed several times with IPA−water mixture (8/1 v/v) to remove remaining salts completely. Finally, the oligomers were dried in a vacuum oven at 120 °C for 24 h. As a next step, we prepared the acSPAES-100 by substituting the hydroxyl end groups of oligomers with the acrylate end groups. The hSPAES-100 (3.33 mmol) was dissolved in anhydrous DMAc (100 mL) at 80 °C. Potassium carbonate, 2.2 equiv based on the sulfonic groups of hSPAES-100, was also dissolved in the solution. After cooling to room temperature, acryloyl chloride (3.33 mmol), 5 equiv based on hydroxyl end groups of hSPAES-100, was added to the solution. The solution was stirred overnight at room temperature under an atmosphere of nitrogen. The reaction compounds were filtrated by glass filter to remove remaining salts and precipitated via coagulation in IPA. Then, to substitute sodium ions of the acrylate-terminated oligomers with tetrabutylammonium ions, tetrabutylammonium hydrogensulfate (TBAH), 2 equiv based on sulfonic groups of hSPAES-100, was also slowly added to the solution. After the substitution was completed, the oligomers were washed and vacuum dried at 60 °C for at least 72 h.

For the preparation of the semi-IPN membranes, acSPAES-100 was mixed with RH-2000 (Radel H2000, Solvay) in a common solvent of DMF, where the blend ratio of acSPAES-100 and RH-2000 was determined to be 1/1 by weight. The solid content in the solution was fixed at 20 wt %. For UV-cross-linking, based on the acSPAES-100 content, 3 wt % of benzoin as a UV initiator and 50 mol % of ethylene glycol dimethacrylate as a cross-linking agent were added to the blend solution. The prepared solution was then cast onto a glass substrate and dried under four different conditions, that is, HT1 (60 °C), HT2 (80 °C), HT3 (120 °C), and HT4 (140 °C), for the purpose of varying the solvent-evaporation temperature, which is expected to affect the phase separation kinetics. After the solvent evaporation, to form cross-linked networks, the membranes were subjected to UV irradiation at 110 °C for 1 h. The UV irradiation was performed using a 160 W medium pressure Hg lamp (352 nm, Sankyo Denki), and the UV intensity at the surface of the membranes was measured to be 4.96 mW/cm^2. All semi-IPN membranes were immersed in a 1 N boiling H_2SO_4 solution for 4 h and subsequently rinsed with deionized water at room temperature for 24 h, where the tetrabutylammonium ions in acSPAES-100 were substituted with protons from H_2SO_4. The thickness of the semi-IPN membranes was measured to be in a range of 100 to 120 μm. The final semi-IPN membranes were noted as sIPN-100.

Characterization. The chemical structure and the number-average molecular weight (M_n) of hSPAES-100 and acSPAES-100 were obtained by ^{1}H NMR (Bruker AMX 500) analysis. The glass-transition temperature (T_g) was measured by a differential scanning calorimeter (TA Instruments Q100) at a heating rate of 10 °C/min. The cross-sectional morphology of semi-IPN membranes was examined by a field emission scanning electron microscope (FE-SEM, Sirion). We prepared the specimens by freezing the membranes and subsequently breaking them in liquid nitrogen. In addition to field emission scanning electron microscopy (FE-SEM, Sirion) measurement, the cross-sectional morphology of membranes with fully hydrated and acid form was examined by a tapping mode atomic force microscope (TM-AFM, Digital Instrument Dimension 3000). The domain size in the membranes was analyzed by an image analyzer (LEICA Qwin Standard). We obtained the surface hydrophilicity of

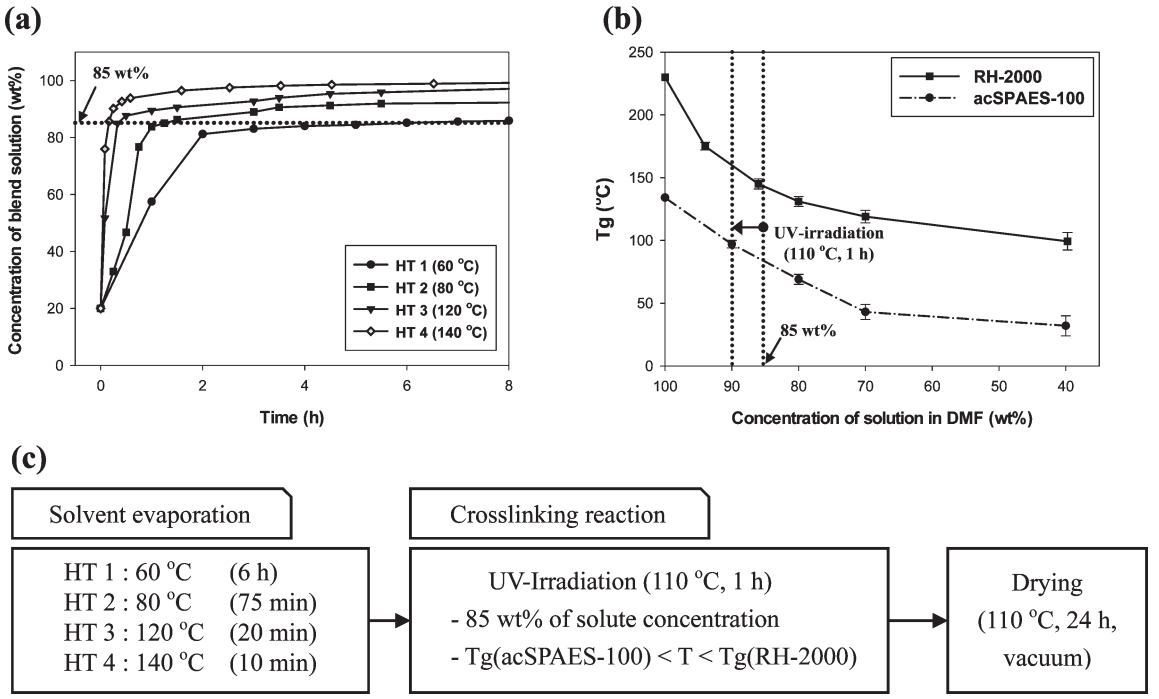

Figure 2. Prerequisite conditions of sIPN-100 preparation for controlling nanoscale phase separation. (a) Concentration change of blend solution with solvent evaporation (a weight-based blend ratio of acSPAES-100 (ammonium form) and RH-2000 in DMF is 1/1). (b) Dependence of T_g on concentration of blend solution. (c) Summary of optimum processing conditions for drying and subsequent UV-cross-linking.

membranes by measuring contact angle toward water (contact angle goniometer, Erma model G-I type). The in-plane proton conductivity was measured by AC impedance spectroscopy technique over a frequency range of 0.1−10 MHz with AC perturbation of 10 mV using a Solatron 1260 impedance/gain-phase analyzer.[17−19] The methanol permeability was measured in an isothermal bath at 25 °C using a two-chamber diffusion cell method with a 2 M methanol solution.[11,17−19]

Results and Discussion

In the ^{1}H NMR spectra (Figure 1), characteristic peaks corresponding to the aromatic protons and the hydroxyl protons of hSPAES-100 (sodium form) as well as acSPAES-100 (ammonium form) were observed. The number-average molecular weight of the oligomers was determined by a ^{1}H NMR end group analysis.[23] By comparing the integration area for protons of the end group BP with that of the main chain BP, the number-average molecular weight of hSPAES-100 was calculated to be 2960 g/mol, which is in close agreement with the initial molecular-design values. Figure 1c shows the successful substitution of the tetrabutylammonium ions as well as the acrylate groups. From the relative integrals of the acrylate end groups and the aromatic resonances, the molecular weight of acSPAES-100 was calculated to be 5870 g/mol. This value is much higher than that of hSPAES-100 because of the bulkier tetrabutylammonium ions as well as the acrylate end groups.

Meanwhile, to determine the optimum conditions for the phase separation kinetics and the UV-cross-linking, a supplementary experiment for the solvent evaporation (Figure 2a) and the T_g measurement (Figure 2b) of the solution was carried out. The morphology of the semi-IPN membranes was developed by two consecutive procedures. The first step is the morphology evolution driven by solvent evaporation, and the second step is the fixation of the preformed morphology by UV-irradiation to create cross-linked networks in the membranes (Figure 2c). Figure 2b shows the upper limit of drying temperatures, which is below the T_g of RH-2000, that is, 150 °C, at a solid content of 85 wt %. Under this drying condition, the RH-2000 phase is a glassy state and immobilizes the acSPAES-100, resulting in the cessation of phase separation. On the basis of these results, the solvent-evaporation conditions were determined to be 60 °C for 6 h (HT1), 80 °C for 75 min (HT2), 120 °C for 20 min (HT3), and 140 °C for 10 min (HT4), where solvent evaporation proceeded until reaching a solid content of 85 wt %.

The prerequisite condition for successful cross-linking of acSPAES-100 is the preservation of the preformed blend morphology. To fulfill this requirement, the cross-linking temperatures were set between the T_g of acSPAES-100 (the rubbery state) and the T_g of RH-2000 (the glassy state) because the cross-linking sites of oligomers need to be mobile enough to contact each other, and at the same time, the preformed morphology should be preserved by the glassy state of RH-2000 phases. As indicated in Figure 2b, the T_g of the blend solution at a solid content of 85 wt % was measured to be 90 °C for the acSPAES-100 and 150 °C for the RH-2000, respectively. On the basis of these observations, the UV-cross-linking temperature was determined to be 110 °C. Prior to the in-depth investigation of the morphology of sIPN-100, to first verify that morphological change during UV-irradiation is not a factor to be considered, the morphology of sIPN-100 before/after UV-irradiation was analyzed. For this study, the membrane prepared under the HT2 drying condition (80 °C, 75 min) and the UV-irradiation condition (110 °C, 1 h) was chosen to be a representative example. Figure 3 shows that before UV-irradiation, the solid content of membranes was 85 wt % and the average domain size appeared to be 50.8 nm. After UV irradiation, the solid content was 90 wt % and the average domain size was 48.5 nm. This verifies that the morphological change during UV-irradiation is negligible and validates the use of UV-irradiation for preparing cross-linking networks in the semi-IPN membranes.

As a first step to understanding the membrane properties of sIPN-100, a ternary phase diagram comprising acSPAES-100 (sodium or ammonium form), RH-2000, and DMF was examined. We determined the cloud point curve by observing the change of the transmitted light intensity during solvent evaporation at 120 °C, that is, the HT3 drying condition as a representative example. As shown in Figure 4a, point A in the phase

diagram indicates a weight-based blend ratio of 1/1, and the curve is a bimodal line, separating the miscible and the immiscible regions. The phase boundary for the ammonium form of acSPAES-100 was formed at a lower solvent concentration, in contrast with that of the sodium form of acSPAES-100. In the sodium form of acSPAES-100, the blend membrane exhibited coarsely phase-separated morphology with large-sized domains, which could even be observed by the naked eye (Figure 4b). In contrast, the membranes with the ammonium form of acSPAES-100 yield a transparent film, evidencing improved miscibility (Figure 4c,d). Because the tetrabutylammoium ions contribute to lowering the hydrophilicity of polar sulfonate groups, the polarity difference between acSPAES-100 and RH-2000 became smaller, and consequently, the cloud points shifted toward the lower solvent concentration. Such a change in the phase diagram forecasts the fact that during the solvent evaporation, the onset of phase separation will be delayed and the morphology may be frozen in an early stage of the phase separation because the viscosity of the blend solution at the low solvent concentration is too high to allow facile motion of the blend components. Therefore, from the phase diagram of acSPAES-100 (ammonium form)/RH-2000/DMF, a cocontinuous morphology with smaller domain size could be expected.

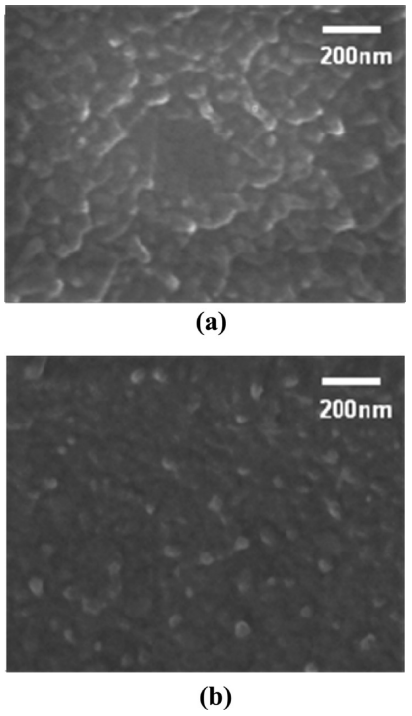

Figure 3. Influence of UV-cross-linking on morphological change of sIPN-100. FE-SEM cross-sectional images of (a) before UV-cross-linking (average domain size is 50.8 nm) and (b) after UV-cross-linking (average domain size is 48.5 nm).

Figure 5 exhibits the cross-sectional morphology of sIPN-100. It can be reasonably expected that as the solvent evaporates, the liquid−liquid phase separation between the acSPAES-100 (ammonium form)-rich phase and the RH-2000-rich phase begins to evolve. As shown in Figure 5a, all of the sIPN-100 showed a cocontinuous morphology, where the domains correspond to the acSPAES-100-rich phases and their sizes vary from 37 to 72 nm, depending on the drying conditions (HT1, HT2, HT3, HT4). In addition, the acSPAES-100-rich domains appeared to be well-connected in a 3D space, which could reflect the fact that the phase separation occurred via spinodal decomposition. To the best of our knowledge, this unique blend morphology characterized by nanoscale domains with well-developed phase cocontinuity has never been explored in conventional blend membranes. It can be reasonably speculated that the delayed onset of phase separation and the freezing of the morphology in the early stage of phase separation in sIPN-100 allowed the formation of this novel morphology.

Meanwhile, it is also of note that as the drying temperature decreased from HT4 to HT1, the phase separation became more delayed, leading to a further decrease in the domain size. In terms of phase separation kinetics, a critical factor for governing the morphology of sIPN-100 is the solvent-evaporation rate, determined by the drying temperature. Lower drying temperature is expected to hinder the chain mobility of the blend components, causing suppression of phase separation. Consequently, a decrease in the drying temperature allowed the cessation of morphological evolution in the earlier stage of phase separation, leading to a further decrease in the domain size.

The morphology of sIPN-100 for the fully hydrated states was investigated using a tapping mode atomic force microscope (TM-AFM), where the scan sizes are 1000 × 1000 and

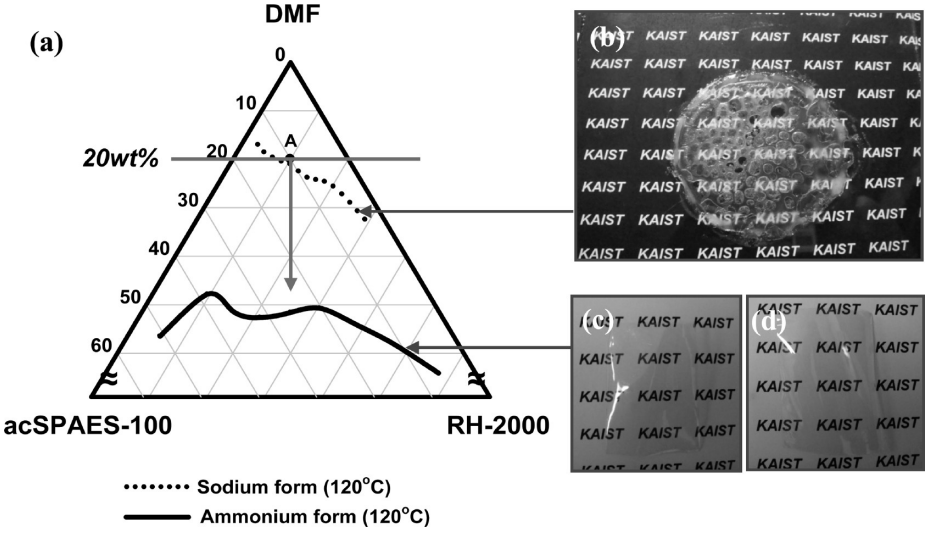

Figure 4. (a) Ternary phase diagram of acSPAES-100 (sodium or ammonium form)/RH-2000/DMF, point A, indicates a weight-based blend ratio of 1/1. Optical images of blends prepared from (b) sodium and (c) ammonium form acSPAES-100, respectively, after drying at 120 °C for 20 min. (d) Optical image of sIPN-100 prepared from ammonium form acSPAES-100 after drying at 120 °C for 20 min and subsequent UV-cross-linking at 110 °C for 1 h.

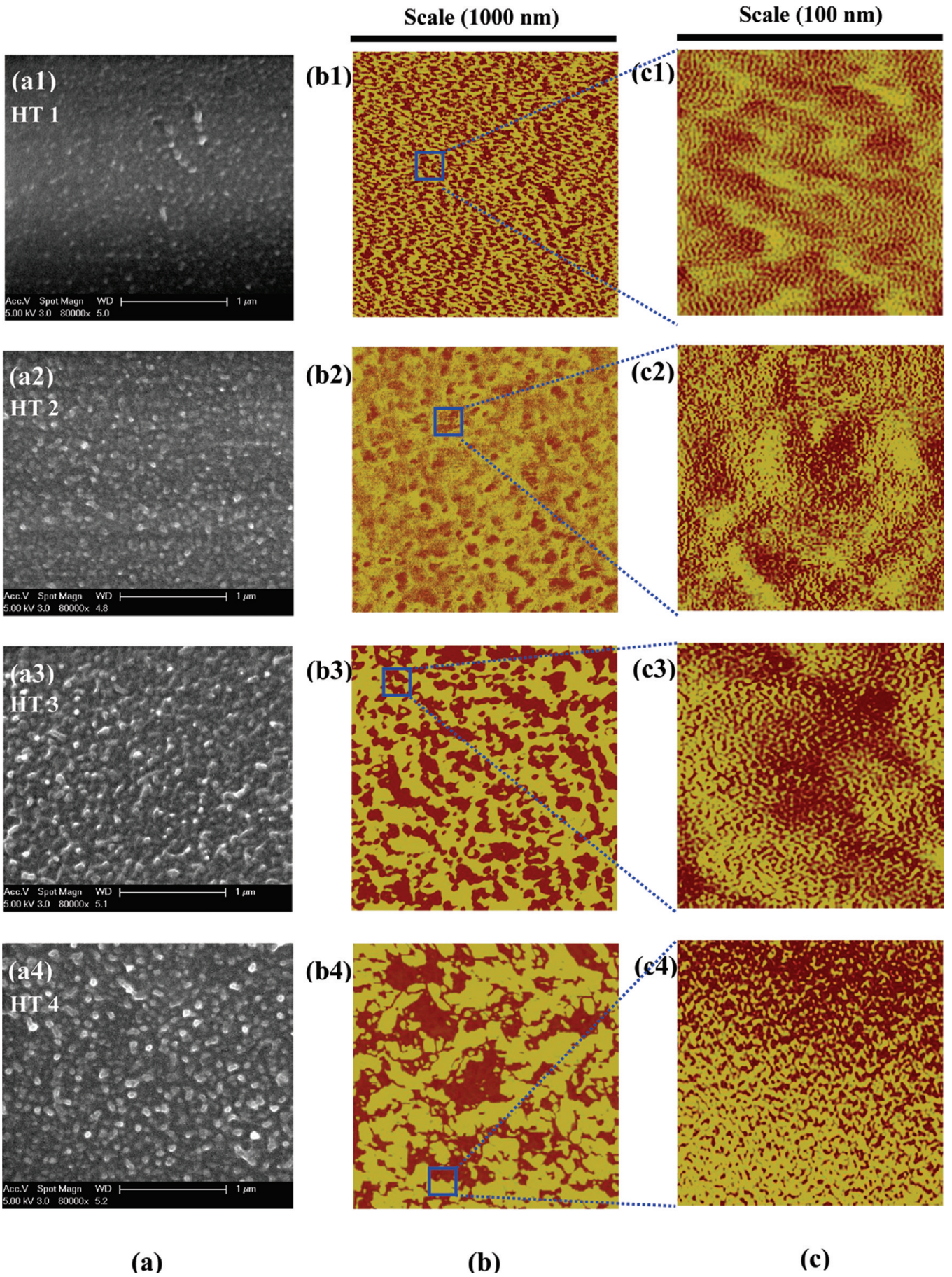

Figure 5. Cross-sectional morphologies of sIPN-100 observed by FE-SEM (dried state) and TM-AFM (fully hydrated state). (a) FE-SEM images (drying condition; average domain size): (a1) HT1, 37 nm; (a2) HT2, 48 nm; (a3) HT3, 63 nm; (a4) HT4, 72 nm. (b) TM-AFM images on 1000 nm scale (drying condition; average hydrophilic domain size): (b1) HT1, 15 nm; (b2) HT2, 26 nm; (b3) HT3, 34 nm; (b4) HT4, 39 nm. (c) TM-AFM images on 100 nm scale (drying condition; average water-channel size): (c1) HT1, 1.2 nm; (c2) HT2, 1.5 nm; (c3) HT3, 2.3 nm; (c4) HT4, 3.0 nm.

Table 1. Summary of Effect of Drying Conditions on Membrane Properties for sIPN-100 (Acid Form) at 25 °C

	nafion	HT1	HT2	HT3	HT4
contact angle (deg)	79.0	66.0	64.0	60.0	55.0
water uptake (wt %)	33.9	15.1	16.4	17.3	18.7
methanol uptake (wt %)	67.3	21.5	22.5	24.1	27.7
proton conductivity (S/cm) (relative value vs nafion)	0.0903 (1.000)	0.0187 (0.207)	0.0170 (0.188)	0.0163 (0.181)	0.0156 (0.173)
methanol permeability ($\times 10^{-8}$ cm^2/s) (relative value, vs nafion)	172.6 (1.000)	2.2 (0.013)	3.3 (0.019)	5.1 (0.030)	7.4 (0.043)
selectivity ($\times 10^4$ S s/cm^3) (relative value vs nafion)	5.2 (1.000)	85.0 (16.346)	51.5 (9.904)	32.0 (6.154)	21.1 (4.058)

100×100 nm^2. It is meaningful to examine the fully hydrated cross sections because this could reflect the actual operation behaviors of DMFC membranes.[17] Figure 5b,c clearly demonstrates that the cocontinuous morphology with an interconnected acSPAES-100-rich phase was developed, which is consistent with previous FE-SEM results and also reflects the fact that the phase separation proceeded through spinodal decomposition. Another interesting observation is that in the 100 nm scan size images, secondary phase separation occurred for both the hydrophilic phase (acSPAES-100-rich phase) and the hydrophobic phase (RH-2000-rich phase). This complex morphology can be explained by considering the fact that even after the primary phase separation, further solvent evaporation may take place, inducing secondary phase separation. Considering previous reports that the water channels of polyelectrolyte membranes are less than 10 nm in size,[24] it can be reasonably concluded that the dark parts in the phase images of 100 nm scan size correspond to the water channels, whereas the dark parts in the phase images of 1000 nm scan size represent the acSPAES-100-rich phases.

Meanwhile, in the phase image of 1000 nm scan size, as the drying temperature was decreased, the acSPAES-100-rich domain size also decreased and the domains became more interconnected as well as less captured inside the RH-2000-rich phases. In general, with spinodal decomposition, the primary morphological features that developed during the earlier stage tend to persist through the whole spinodal decomposition. However, when rapid growth of sinusoidal composition modulation continues to proceed, a morphology with isolated domains could develop through the coalescence of new phases generated by nucleation and growth.[17] Therefore, at high drying temperatures that allow a decrease in the medium viscosity and thus facilitate phase separation, the acSPAES-100-rich domains become larger and more isolated. Furthermore, in the phase images of 100 nm scan size (Figure 5c), it was also observed that as the drying temperature decreased, the average size of the water channels in the acSPAES-100-rich domains decreased, reducing to 1.2 to 3.0 nm, and the phase cocontinuity was more developed.

Table 1 shows the effect of drying temperature (i.e., the effect of morphological change) of sIPN-100 on the DMFC membrane properties at 25 °C. As the drying temperature was decreased, the water uptake and the methanol uptake of sIPN-100 become lowered. In addition, the contact angle, which reflects the surface hydrophilicity, was also increased. These interesting observations indicate that cocontinuous morphology with nanoscale domains could effectively prevent the membranes from absorbing water, rendering them more hydrophobic. As a supplementary experiment, the water uptake and the methanol uptake of a cross-linked polymer (x-acSPAES-100), which is synthesized from pristine acSPAES-100 alone without being blended with RH-2000, were examined and observed to be 492 and 527%, respectively. From a comparison between pristine x-acSPAES-100 and sIPN-100, it is apparent that the introduction of a semi-IPN structure has a remarkable effect in terms of reducing the water uptake (492 → 15.1%) and the methanol uptake (527 → 21.5%).

The proton conductivity of sIPN-100 was measured in a temperature range from 25 to 70 °C (Figure 6a). Consistent with previous reports,[10−20] the proton conductivity of sIPN-100

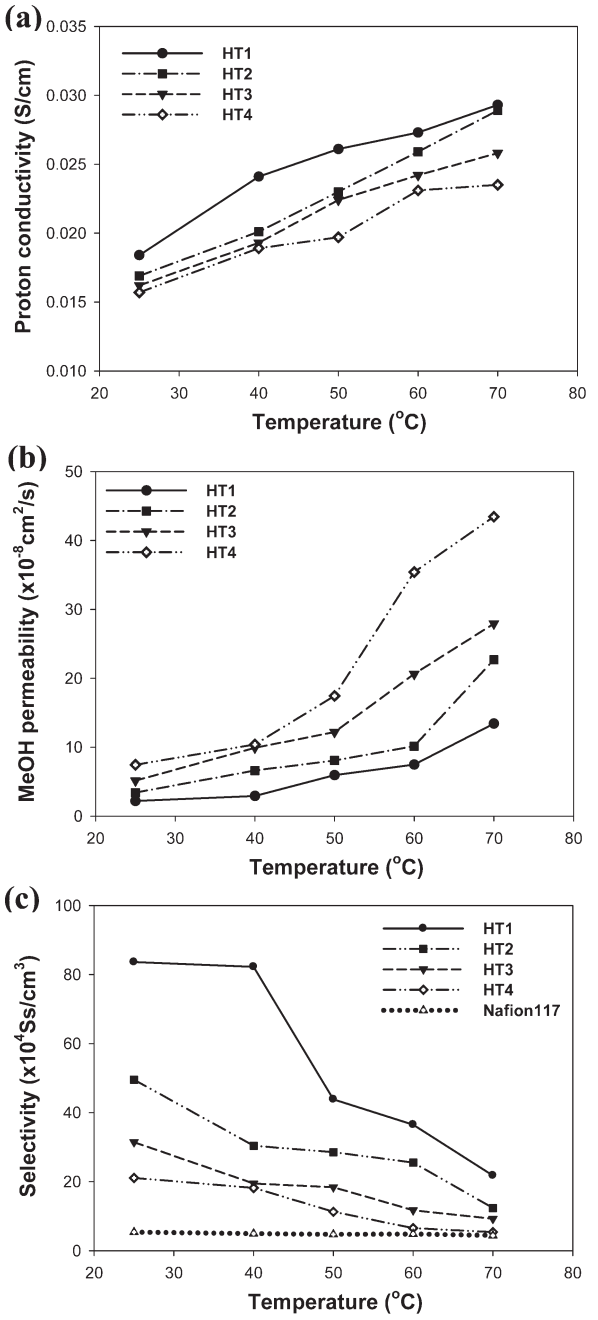

Figure 6. Effect of drying conditions on membrane transport properties of sIPN-100. (a) Proton conductivity. (b) Methanol permeability. (c) Selectivity. The membrane prepared at the HT1 drying condition demonstrates the highest selectivity, which is approximately 16 times higher than that of Nafion117.

increased in proportion to the increase in the measuring temperature. An interesting observation is that at the same measuring temperature, as the drying temperature decreases, that is, the size of acSPAES-100-rich domains decreases, the proton conductivity tends to increase. This seems to be contrary to the expectation

based on the results of water uptake because proton conductivity generally tends to increase with an increase in water uptake.[15,25,26] Previous publications on the blend membranes reported that a decrease in the domain size lowered the water uptake, leading to a decrease in the proton conductivity.[16−19] The unique behavior of proton conductivity in sIPN-100 can be explained by considering the domain size and the phase cocontinuity rather than the water uptake alone. Previous observations of sIPN-100 confirmed that as the drying temperature is decreased, the domain size decreased and better phase cocontinuity was developed. This morphological change may contribute to providing a shorter tortuous path of proton transport, which is expected to have a positive effect on the proton conductivity. At the same time, the water uptake was lowered because of a decrease in the hydrophilicity. These results suggest that the proton conductivity of sIPN-100 could be determined by two competing factors, that is, the morphology and the water uptake. Figure 6a verifies the fact that the well-developed phase cocontinuity with nanometer-sized hydrophilic domains played a more dominant role in determining the proton conductivity than the water uptake.

Figure 6b demonstrates that as the drying temperature is decreased, that is, the hydrophilic domain size decreased, the methanol crossover becomes suppressed, which is consistent with the decrease of water uptake and methanol uptake shown in Table 1. In general, the methanol transport properties of fuel cell membranes greatly depend on the fraction of free water.[19,20] It was previously observed that lower drying temperature caused a decrease in the domain size, which contributed to increasing hydrophobicity. Consequently, a decrease in the drying temperature is expected to lower the fraction of free water within the membranes. In addition, the well-connected, hydrophobic RH-2000-rich phases could hinder the methanol from passing through the membranes and also suppress the expansion of hydrophilic phases. Therefore, it is suggested that both the decreased domain size and the well-developed phase cocontinuity make it possible to suppress methanol crossover of sIPN-100.

The selectivity, that is, the ratio of proton conductivity to methanol permeability, is a crucial factor for governing DMFC membrane performance. Accordingly, higher selectivity could allow superior DMFC membrane performance. From Figure 6c, it is seen that relative to Nafion117, sIPN-100 showed a dramatic improvement in selectivity. A more detailed comparison of sIPN-100 with Nafion117 in terms of transport properties was summarized in Table 1. As a representative example, the sIPN-100 prepared under the HT1 drying condition was compared with Nafion117. The proton conductivity at 25 °C was measured to be 0.0187 S/cm for sIPN-100 at the HT1 and 0.0903 S/cm for Nafion117, respectively. In contrast, the methanol permeability of sIPN-100 at the HT1 was much lower than that of Nafion117, that is, 2.2×10^{-8} for sIPN-100 and 172.6×10^{-8} cm^2/s for Nafion117. This comparison reveals that for sIPN-100, the reduction of methanol permeability is much greater than that of proton conductivity, contributing to higher selectivity. Meanwhile, among the sIPN-100 samples, the membrane prepared under the HT1 drying condition showed the highest selectivity, being approximately 16 times higher than that of Nafion117. It was already observed that as the drying temperature was decreased, sIPN-100 presented smaller hydrophilic domain size and better phase cocontinuity. The enhancement in the selectivity is thought to be attributable to this morphological change.

Conclusions

In summary, we developed nanometer-sized domains and well-established phase cocontinuity of sIPN-100 by controlling the kinetics as well as the thermodynamics of nanoscale phase separation. The introduction of acSPAES-100 oligomers with low molecular weight and low hydrophilicity made it possible to shift the boundary of phase separation to a low concentration of solvent in the phase diagram and to restrict the phase separation of sIPN-100. The solvent-evaporation temperatures also played an important role in governing the phase separation kinetics. The lower solvent-evaporation temperature contributed to a further decrease in the hydrophilic domain size and the better phase cocontinuity. This morphological change rendered sIPN-100 more hydrophobic and effectively lowered the water uptake, the methanol uptake, and the surface hydrophilicity. It is worthwhile to note that the novel morphology of sIPN-100 allowed unique behaviors of proton conductivity and methanol permeability, which have previously not been seen in microscale phase separation. More notably, sIPN-100 demonstrated significant improvement in selectivity that is not likely to be attained via conventional approaches.

Acknowledgment. We are grateful to Dr. Y. T. Hong at KRICT for his kind discussion on the characterization of DMFC membrane transport properties.

References and Notes

(1) Baradie, B.; Poinsignon, C.; Sanchez, J. Y.; Piffard, Y.; Vitter, G.; Bestaoui, N.; Foscallo, D.; Denoyelle, A.; Delabouglise, D.; Vaujany, M. *J. Power Sources* **1998**, *74*, 8–16.
(2) Wang, F.; Hickner, M.; Ji, Q.; Harrison, W.; Mecham, J.; Zawodzinski, T. A.; McGrath, J. E. *Macromol. Symp.* **2001**, *175*, 387–396.
(3) Wang, F.; Hickner, M.; Kim, Y. S.; Zawodzinski, T. A.; McGrath, J. E. *J. Membr. Sci.* **2002**, *197*, 231–242.
(4) Bishop, M. T.; Karasz, F. E.; Frank, E.; Russo, P. S.; Langley, K. H. *Macromolecules* **1985**, *18*, 86–93.
(5) Kobayashi, T.; Rikukawa, M.; Sanuia, K.; Ogata, N. *Solid State Ionics* **1998**, *106*, 219–225.
(6) Gebel, G.; Aldebert, P.; Pineri, M. *Polymer* **1993**, *34*, 333–339.
(7) Li, Q.; He, R.; Jensen, J. O.; Bjerrum, N. J. *Chem. Mater.* **2003**, *15*, 4896–4915.
(8) Kreuer, K. D. *Solid State Ionics* **1997**, *97*, 1–15.
(9) Kreuer, K. D. *J. Membr. Sci.* **2001**, *185*, 29–39.
(10) Lee, S. Y.; Scharfenberger, G.; Meyer, W. H.; Wegner, G. *Adv. Mater.* **2005**, *17*, 626–630.
(11) Lee, C. H.; Min, K. A.; Park, H. B.; Hong, Y. T.; Jung, B. O.; Lee, Y. M. *J. Membr. Sci.* **2007**, *303*, 258–266.
(12) Colicchio, I.; Keul, H.; Simon, U.; Weirich, T. E.; Moeller, M. *Fuel Cells* **2006**, *3*, 225–236.
(13) Oh, Y. S.; Lee, H. J.; Yoo, M. J.; Kim, H. J.; Han, J. H.; Kim, T. H. *J. Membr. Sci.* **2008**, *323*, 309–315.
(14) Lei, L.; Zhang, J.; Wang, Y. *J. Mater. Sci. Letters* **2003**, *22*, 1595–1597.
(15) Dai, C. A.; Liu, C. P.; Lee, Y. H.; Chang, C. J.; Chao, C. Y.; Cheng, Y. Y. *J. Power Sources* **2008**, *177*, 262–272.
(16) Kerres, J. A. *J. Membr. Sci.* **2001**, *185*, 3–27.
(17) Kim, D. H.; Choi, J. S.; Hong, Y. T.; Kim, S. C. *J. Membr. Sci.* **2007**, *299*, 19–27.
(18) Choi, J. S.; Kim, D. H.; Kim, H. K.; Shin, C. K.; Kim, S. C. *J. Membr. Sci.* **2008**, *310*, 384–392.
(19) Kim, D. H.; Kim, S. C. *Macromol. Res.* **2008**, *16*, 457–466.
(20) Harrison, W. L.; Hickner, M. A.; Kim, Y. S.; McGrath, J. E. *Fuel Cells* **2005**, *2*, 201–212.
(21) Olabisi, O.; Robeson, L. M.; Shaw, M. T. *Polymer−Polymer Miscibility*; Academic Press: New York, 1979.
(22) Paul, D. R.; Newmans, S. *Polymer Blends*; Academic Press: New York, 1978.
(23) Lee, H. S.; Roy, A.; Lane, O.; Duun, S.; McGrath, J. E. *Polymer* **2008**, *49*, 715–723.
(24) Mauritz, K. A.; Moore, R. B. *Chem. Rev.* **2004**, *104*, 4535–4586.
(25) Kim, Y. S.; Sumner, M. J.; Harrison, W. L.; Riffle, J. S.; McGrath, J. E.; Pivovar, B. S. *J. Electrochem. Soc.* **2004**, *151*, A2150–A2156.
(26) Wang, Z.; Li, X.; Zhao, C.; Ni, H.; Na, H. *J. Appl. Polym. Sci.* **2007**, *104*, 1443–1450.